

Many-body computing on Field Programmable Gate Arrays

Songtai Lv (吕松泰),^{1,*} Yang Liang (梁洋),^{2,*} Yuchen Meng (孟雨晨),¹ Xiaochen Yao (姚晓晨),² Jincheng Xu (徐锦程),² Yang Liu (刘洋),¹ Qibin Zheng (郑其斌),^{2,†} and Haiyuan Zou (邹海源)^{1,‡}

¹Key Laboratory of Polar Materials and Devices (MOE),

School of Physics and Electronic Science, East China Normal University, Shanghai 200241, China

²Laboratory of Radiation Detection and Medical Imaging, School of Health Science and Engineering, *University of Shanghai for Science and Technology, Shanghai 200093, China*

A new implementation of many-body calculations is of paramount importance in the field of computational physics. In this study, we leverage the capabilities of Field Programmable Gate Arrays (FPGAs) for conducting quantum many-body calculations. Through the design of appropriate schemes for Monte Carlo and tensor network methods, we effectively utilize the parallel processing capabilities provided by FPGAs. This has resulted in a remarkable tenfold speedup compared to CPU-based computation for a Monte Carlo algorithm. We also demonstrate, for the first time, the utilization of FPGA to accelerate a typical tensor network algorithm. Our findings unambiguously highlight the significant advantages of hardware implementation and pave the way for novel approaches to many-body calculations.

keywords: Many-body physics, FPGA, Monte Carlo, Tensor networks

I. INTRODUCTION

Many-body computations are a pivotal research focus within the fields of condensed matter and statistical physics. These computations employ sampling methods, such as classical and quantum Monte Carlo (MC) [1], as well as blocking methods like Density Matrix Renormalization Group [2] and tensor networks [3, 4]. Traditionally, the central processing unit (CPU) of a general-purpose computer based on the von Neumann architecture, along with the graphics processing unit (GPU) used for parallel processing, are typical means of implementing many-body calculations. However, certain bottleneck issues, such as the critical slowdown observed in calculations at the vicinity of a phase transition point, persist. Therefore, exploring additional parallel approaches or strategies for many-body computations is imperative to overcome these challenges.

Besides from the algorithmic point of view, an alternative approach is to optimize the computations from a hardware perspective. Taking the von Neumann architecture as the first reference example, a typical CPU follows a five-stage instruction execution process consisting of Instruction Fetch (IF), Instruction Decode (ID), Execution (EX), Memory Access (MEM), and Write Back (WB) [5][Fig. 1(a)]. Moreover, instructions and data are stored in the same memory, which creates a bottleneck [6] in performance due to the data transfer rate limitation between the processor and memory. Meanwhile, the CPU frequency in the GHz range is difficult to substantially improve due to physical limitations [7]. These bottlenecks significantly discount the parallel performance of the CPU. For instance, although supercomputers feature

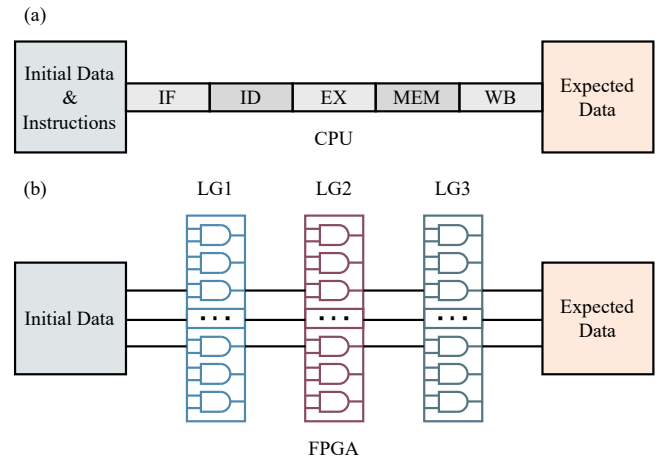


FIG. 1. The architectural differences between FPGA and CPU. (a) In the case of CPU, initial data and instructions are stored in the same memory, and after passing through stages of Instruction Fetch (IF), Instruction Decode (ID), Execution (EX), Memory Access (MEM), and Write Back (WB), the expected data is computed. (b) In FPGA, instructions are implemented by constructing logic gates (LGs), and initial data flows through several LGs to generate the expected data.

multiple parallel processing units, increasing parallelism does not always lead to linear performance growth.

In general, one can improve computational efficiency by modifying or abandoning the von Neumann architecture, but this may come at the cost of losing flexibility. For example, GPUs introduce Single Instruction, Multiple Threads or Single Instruction, Multiple Data execution modes to improving parallelism. However, the execution process still require the IF, ID, and EX stages. Therefore, we categorize GPUs as hardware approximating the von Neumann architecture. In contrast, an application-specific integrated circuit (ASIC)

* These authors contributed equally to this study.

† qbzheng@usst.edu.cn

‡ hyzou@phy.ecnu.edu.cn

is designed to perform specific tasks, while losing versatility at the hardware level, but making them highly efficient. For instance, the specialized Tensor Processing Units (TPUs) can significantly accelerate the simulation of quantum many-body dynamic problems [8]. Between the extreme cases of CPU/GPU and ASIC, a Field-Programmable Gate Array (FPGA) can also execute computational tasks in parallel at the hardware level by arranging the computational instructions into logic gates [Fig. 1(b)]. Take a loop operation for example, FPGAs can utilize pipeline architecture to accelerate the operation by breaking down the computational tasks of each iteration into multiple stages. These stages are executed concurrently in parallel, allowing for overlapping computation and data transfer, which significantly reduces the overall latency. Meanwhile, the structure maintains considerable versatility, as its logic gates are reconfigurable.

Possessing valuable properties such as high throughput, high energy efficiency, and the capacity to maximize parallelism, FPGAs have emerged as versatile platforms in numerous fields, including quantum chemistry [9], neural networks [10], high-energy physics [11], etc. For example, in a high-energy physics experiment, FPGAs process vast amounts of data from particle detectors, aiding in the analysis of particle collections and collisions [11]. Interestingly, the structure of the FPGA has even been implemented in a biological system [12]. Although FPGAs have found extensive application in these fields, their utilization in many-body computations is primarily confined to integer-variable spin models like the various Ising models [13–16]. The substantial parallel advantages of FPGAs have not been fully exploited in the realm of many-body systems with more degrees of freedom, particularly in the area of tensor networks.

Here, we implement two typical many-body algorithms on FPGA, utilizing the two-dimensional (2D) XY model and the one-dimensional (1D) Heisenberg chain as examples. Using only a single FPGA chip, we showcase its significant parallel acceleration capabilities (The details of the chip are shown in the Appendix). First, we construct a parallel scheme for the Metropolis MC updating procedure of the two-dimensional classical XY model, achieving a tenfold speedup compared to the CPU. Second, we restructure the Infinite Time-Evolving Block Decimation (iTEBD) [17], a typical tensor network algorithm, making it suitable for hardware execution and also beating the CPU speed for the first time. Our work has achieved hardware FPGA acceleration for many-body computations, offering a novel approach to this field in general.

The rest of this work are outlined as follows: Section II introduces the necessary modifications to the Metropolis Monte Carlo and iTEBD algorithms for hardware acceleration. Section III shows the acceleration performance of FPGA. Lastly, Section IV provides discussions and a summary.

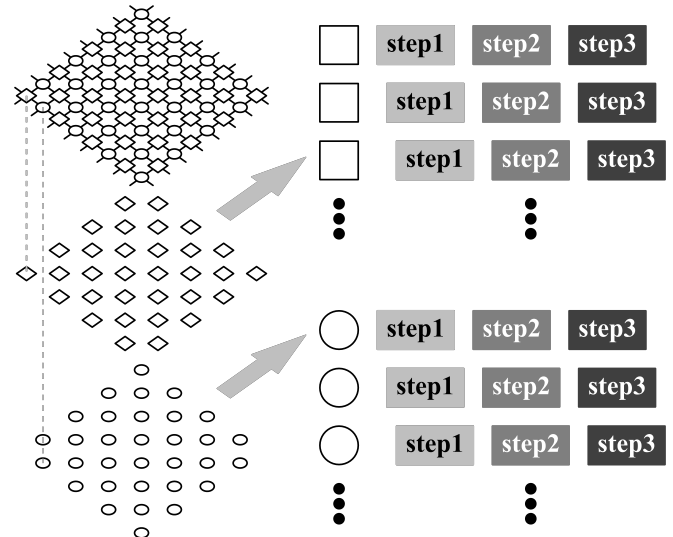


FIG. 2. Sublattice decomposition and pipeline parallel computation of the XY model on the square lattice. The left side depicts two sublattices distinguished by square and circular patterns. The right side illustrates each sublattice's evolution processes, consisting of three steps: Step 1 generates the initial state, Step 2 calculates the probability of transitioning to a new state, and Step 3 determines whether the transition occurs. Each step can be computed in parallel using pipelining on FPGA.

II. MODELS AND METHODS

In FPGAs, instructions to fulfill a certain algorithm are not like the instruction sets in traditional CPUs. Instead, they are actually descriptions of logical circuit structures and functionalities tailored to the algorithm. Hardware description languages are used to articulate the desired logical circuit functions and behaviors. Subsequently, FPGA development tools synthesize these descriptions into logic netlists and generate bitstream files, which are then loaded into FPGA devices for computation. It is worth noting that utilizing new hardware like FPGA for computations does not diminish the importance of algorithms. On the contrary, algorithms remain crucial, and it is essential to modify algorithms suitable for parallel execution on FPGA to fully leverage its parallel processing capabilities. In this section, we modify algorithms suitable for parallel execution on FPGA for Metropolis Monte Carlo and iTEBD computations, using the 2D XY model and the 1D Heisenberg chain as examples, respectively.

A. Parallel design of MC simulation for the XY model

We first focus on the 2D classical XY model, which is renowned for the Kosterlitz-Thouless phase transi-

tion [18] and is described by the following Hamiltonian:

$$H_{XY} = - \sum_{(\mathbf{x}, \delta)} \cos(\theta_{\mathbf{x}} - \theta_{\mathbf{x}+\delta}) \quad (1)$$

where \mathbf{x} denotes a site on the square lattice, δ is a unit vector connecting this site with one of its nearest neighbours and the variable $\theta_{\mathbf{x}} \in [0, 2\pi)$ represents the direction of the spin at site \mathbf{x} .

We employ the straightforward Metropolis algorithm to evolve the configurations of the system. Due to bipartition of the square lattice, half of the spins can be evolved independently and in parallel. Therefore, we divide the lattice system into two sets of subsystems and update them alternately (as illustrated in Fig. 2) by following the approach used in Ref. [13]. In each subsystem, the MC procedure is further divided into three steps. First, random parameters are generated for each spin as the initialization of the Metropolis process. Second, the local internal energy difference caused by spin flipping is calculated, and the probability of flipping is determined. Third, a probabilistic decision to finish the Metropolis process is made, and the spin states are updated. More details of the Metropolis process are provided in the Appendix.

During the evolution process for each subsystem, the iterative step for each spin can be unrolled, thereby avoiding the serial iteration of independent steps and fully utilizing available hardware resources for acceleration. After implementing the entire MC algorithm into the FPGA hardware, we can readily employ the pipeline architecture to accelerate the computation. We calculate the energy of the system and obtain results consistent with those from CPUs (details shown in the Appendix). The computational speed advantage of FPGA compared to CPUs is demonstrated in the Results section.

B. Parallel design of iTEBD for the Heisenberg chain

We then demonstrate the implementation of the iTEBD algorithm on FPGA for the 1D antiferromagnetic Heisenberg model. The Hamiltonian for this model is as follows:

$$H_H = \sum_{\langle ij \rangle} H_{ij} = \sum_{\langle ij \rangle} S_i^x S_j^x + S_i^y S_j^y + S_i^z S_j^z, \quad (2)$$

where the interaction H_{ij} is applied locally between the nearest neighbor sites i and j , and $S_i^\mu = \sigma^\mu/2$, with σ^μ being the three Pauli matrices ($\mu = x, y, z$).

In the usual iTEBD setup, the initial wavefunction $|\Psi\rangle$ of the system is constructed as $|\Psi\rangle = \dots \lambda_{2,ij} A_{jk}^\alpha \lambda_{1,kl} B_{lm}^\beta \lambda_{2,mp} \dots |\dots \alpha\beta \dots\rangle$, where A, B , and $\lambda_{1,2}$ are local tensors, and all the virtual indices i, j , etc are contracted. These ingredients are updated by local imaginary time evolution $|\tilde{\Psi}\rangle = \prod_{\langle ij \rangle} U_{T,ij} |\Psi\rangle =$

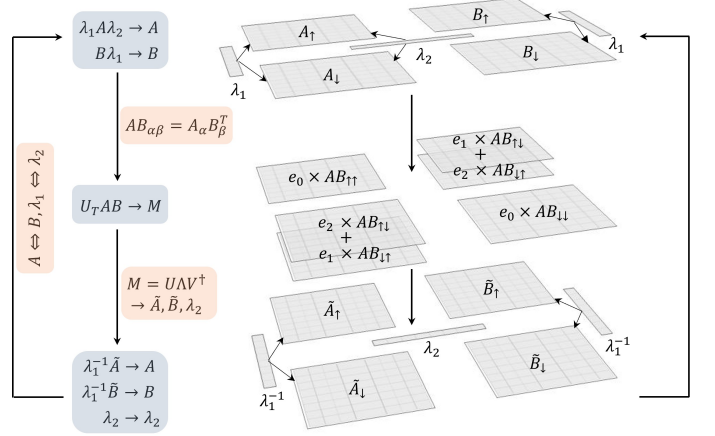


FIG. 3. Schematic diagram of the iTEBD calculation for the Heisenberg model: the left side depicts the variable flowchart, while the right side shows the corresponding matrix representations. The iTEBD process consists of three steps: First, after multiplying λ_1 and λ_2 into A_1 , A_2 , B_1 , and B_2 , A and B are directly multiplied to obtain the matrix. Second, AB undergoes evolution through gate U_T to yield M , and SVD is applied to M to obtain matrices U , Λ , and V , which are truncated to dimension D_b to generate \tilde{A} , \tilde{B} , and λ_2 . Third, λ_1^{-1} is multiplied into \tilde{A} , \tilde{B} to obtain the new A and B for the next iteration of the iTEBD process.

$\prod_{\langle ij \rangle} e^{-\tau H_{ij}} |\Psi\rangle$ until convergence, where the local gate U_T has a matrix representation

$$U_T = \begin{pmatrix} e_0 & 0 & 0 & 0 \\ 0 & e_1 & e_2 & 0 \\ 0 & e_2 & e_1 & 0 \\ 0 & 0 & 0 & e_0 \end{pmatrix} \quad (3)$$

with the bases $\{|\uparrow\uparrow\rangle, |\uparrow\downarrow\rangle, |\downarrow\uparrow\rangle, |\downarrow\downarrow\rangle\}$, and the nonzero elements of U_T are $e_0 = \langle \uparrow\uparrow | e^{-\tau H_{ij}} |\uparrow\uparrow \rangle = \langle \downarrow\downarrow | e^{-\tau H_{ij}} |\downarrow\downarrow \rangle$, $e_1 = \langle \uparrow\downarrow | e^{-\tau H_{ij}} |\uparrow\downarrow \rangle = \langle \downarrow\uparrow | e^{-\tau H_{ij}} |\downarrow\uparrow \rangle$, $e_2 = \langle \uparrow\downarrow | e^{-\tau H_{ij}} |\downarrow\uparrow \rangle = \langle \downarrow\uparrow | e^{-\tau H_{ij}} |\downarrow\uparrow \rangle$. In our calculation, the length of on time step τ is set as $\tau = 0.01$. Moreover, in the evolution process, it is necessary to utilize singular value decomposition (SVD) approximation to ensure that the virtual bond dimension is fixed as a finite value D_b .

When performing tensor network computations on CPUs, tensors or matrices are often defined as classes. This allows for intuitive and crucial operations like permutation and reshaping of the classes themselves when contracting tensors with different indices. These operations enhance the intuitiveness and efficiency of tensor operations. However, in the existing FPGA architecture, the input and output data ultimately manifest in the tensor elements themselves. Operations like permutation and reshaping of tensors, which are suitable for CPUs, instead significantly slow down computation speed and increase unnecessary resource consumption on FPGAs. Therefore, in FPGA implementation, one needs to mod-

ify the iTEBD algorithm from the perspective of tensor elements rather than classes. Following this principle, we redesign the iTEBD algorithm suitable for parallel execution on FPGAs (Fig. 3), avoiding excessive tensor operations. For instance, instead of relying on the third-order tensor A_{ij}^α , we employ two matrices A_\uparrow and A_\downarrow , significantly simplifying the process and enabling parallelism. A detailed discussion on the equivalence of this new form with the original iTEBD can be found in the Appendix.

In the iTEBD process, separated by the SVD step, the entire procedure is structured into three stages (Fig. 3): pre-SVD, SVD, and post-SVD. In the pre-SVD stage, λ s are multiplied into matrices A_\uparrow , A_\downarrow , B_\uparrow and B_\downarrow , followed by the multiplication of A s and B s to derive a new matrix AB by $AB_{\alpha\beta} = A_\alpha B_\beta^T$ (α, β can be \uparrow or \downarrow). Subsequently, the non-zero matrix elements of U are used to reassemble AB . In the SVD stage, the reassembled AB undergoes SVD using a parallelizable two-sided Jacobi algorithm (detail in the Appendix). In the post-SVD stage, the obtained results are truncated to preserve the dimension D_b , resulting in new matrices A , B , and λ s. These newly derived matrices are reintegrated into the initial step, facilitating the iterative process until convergence. Using the wavefunction from these process, we get convergent ground state energy consistent with the exact solution for Heisenberg chain (details shown in the Appendix). The computational speed advantage of FPGA compared to CPU is shown in the next section.

III. RESULTS

In this section, we compare the computational time results on CPU and FPGA for both MC simulation for the XY model and iTEBD calculation for the Heisenberg model, showcasing the significant acceleration achieved by FPGA. The same set of modified MC and iTEBD algorithms are deployed across three different platforms: CPU, FPGA in sequential style, and FPGA in pipelined parallel style. For the first two platforms, the simulations were designed in a completely sequential manner. We then measured the computation time of one MC step and one iTEBD step for all cases.

In the MC simulations for the XY model, we executed 10,000 MC steps for five different sizes $L = 8, 16, 32, 64$, and 128 on each platform to measure the average computation time. The results are displayed in Fig. 4(a). While the computational speed of the FPGA in sequential style is slower than that of the CPU, significant speed improvement is achieved with the FPGA in pipelined parallel style. For example, at the system size $L = 128$, the computation speed of the FPGA in parallel is 16.5 times that of the CPU, and 27.3 times that of the FPGA in sequential style. As L increases, the computation time on all three platforms is approximately proportional to L^2 , with slight variations.

Figure 4(b) illustrates the computation time of one

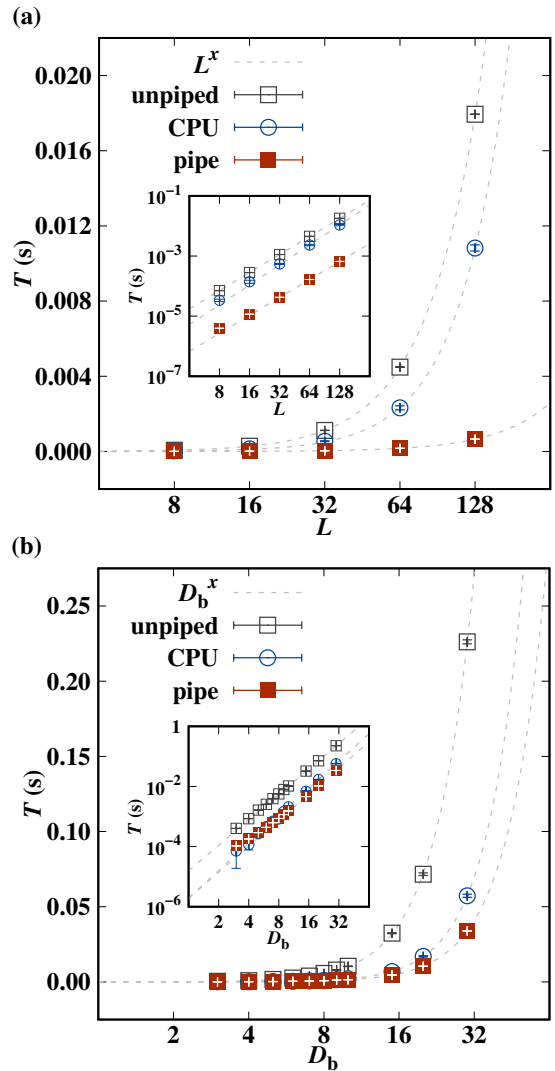


FIG. 4. The computational time per step for (a) MC simulation of the XY model and (b) iTEBD calculation of the Heisenberg chain. The red solid squares, black hollow squares, and blue hollow circles represent the computational time for FPGA in pipelined parallel style, FPGA in sequential style (unipiped), and CPU, respectively. The error bars indicate a 95% confidence interval. The gray dashed lines represent the fitted results of the computational time with the fitting function X^x , where x is the fitting parameters, and $X = L$ or D_b for (a) or (b). In (a), the fitted results for x for FPGA in parallel style, FPGA in sequential style, and CPU are 1.99, 2, and 2.2, respectively. In (b), the corresponding values of x are 2.88, 2.82, and 3.02. The inserts illustrate the corresponding data in log-log scale.

iTEBD step for the Heisenberg chain system. Starting from several fixed initial states, we executed 10,000 to 100,000 iteration steps for 11 different bond dimensions $D_b \leq 30$, aiming to achieve convergent final states with the same level of precision. Similar to the MC simulation, the FPGA in sequential calculations takes the longest time compared to the other two platforms, while

the computational speed of FPGA in parallel surpasses that of the CPU. However, the acceleration effect is not as pronounced as that of the MC calculations. For instance, at $D_b = 30$, the computation speed of the FPGA in parallel is 1.7 times that of the CPU and 6.7 times that of the FPGA in sequential style. Nevertheless, this result remains encouraging because the computation time on FPGA in parallel increases slower with D_b compared to CPU. This suggests the potential for achieving more pronounced acceleration with larger D_b .

Although in both the MC and iTEBD cases, the CPU may outperform the FPGA in sequential, the parallelization effect on an FPGA generally results in higher computational efficiency than the CPU. Compared to the parallelism of CPUs, which mainly relies on multi-core processors and faces issues such as communication and synchronization overheads, as well as shared memory access conflicts, the parallelization on FPGA is much more efficient.

From Fig. 4, it can be observed that the error in the runtime of the FPGA in parallel is smaller compared to the CPU for both the MC and the iTEBD calculation. This highlights another advantage of FPGA: deterministic latency. This is attributed to the architectural differences between the two platforms. When executing complex tasks on the CPU, rescheduling, instruction fetching, decoding, and other operations introduce variability in the runtime for each execution. However, due to its hardware programmability, each operation in an FPGA is fixed within a clock cycle, resulting in smaller runtime errors compared to the CPU.

IV. DISCUSSIONS AND CONCLUSIONS

While the ultimate solution to the exponential wall problem in many-body systems will eventually rely on quantum computers [19], the full utilization of classical algorithms and hardware remains meaningful at present. Generally, the time complexity for computing many-body systems follows a growth pattern of hX^a , where X represents the controllable degrees of freedom for the particular problem, such as system size L in Monte Carlo simulations or bond dimension D_b in tensor network calculations. Improvements in algorithms are reflected in the reduction of a , while hardware parallel optimization alters h . Therefore, comprehensive improvements in both algorithms and hardware will contribute to the efficiency of many-body computations.

For the case of iTEBD calculations in this paper, our primary goal is to implement a tensor network parallel algorithm on FPGA. Therefore, we have focused on avoiding tensor reshaping and permutation operations at the algorithmic level and have only employed pipeline parallelism at the hardware level. However, the most time-consuming aspect of tensor calculations is the SVD process. With improvements in hardware programming for the SVD process, such as utilizing modified systolic

arrays [20] and Coordinate rotation digital computer (CORDIC)-like technology [21] that are better suited for FPGA architectures, the computational speed of tensor network algorithms on FPGA will be significantly enhanced.

Another aspect worth discussing is the current limitations of resources on FPGA chips. For example, although the Block Random Access Memory (BRAM) of the chip we are using is only 15.6Mb (details of the hardware is shown in the Appendix), it can handle many-body problems of moderate scale for L or D_b . However, in tensor network computations, models involving sign problems [22] and the competition of various phases [23, 24] require larger D_b , and solving these problems requires FPGAs with larger memory. The success of TPU [8] on tensor network calculations demonstrates that this is not a technically insurmountable problem. Therefore, optimizing multi-body computations on FPGAs can stimulate the development of chip hardware.

In summary, we have employed FPGA to achieve hardware acceleration for two distinct many-body computation methods. In the MC evolution of the 2D classical XY model, subsystem parallelization significantly boosts the evolution speed, crucial for mitigating issues related to critical slowdown. In the iTEBD tensor network calculation the 1D Heisenberg chain, we have devised a structure optimized for hardware dataflow, streamlining computational steps based on tensor elements. This structural optimization, combined with parallelization, results in speeds surpassing those attainable on a CPU. Notably, this represents the first FPGA implementation of a tensor network algorithm. Our findings offer a novel perspective on many-body computations, fostering interdisciplinary collaboration between the fields of many-body algorithms and hardware.

V. ACKNOWLEDGMENTS

We thank Jianguo Ma, Deyan Sun for helpful discussions. This work is supported by National Natural Science Foundation of China Grant (No. 12274126, 12105177) and National Key R&D Program of China (No. 2023YFF0719200).

VI. APPENDIX

A. Detail of the FPGA and CPU hardware

The FPGA chip model used in this work is XC7K325TFFG900-2. The driving pulse period is 10ns, corresponding to a frequency of 0.1GHz. This chip has 890 Block RAM (BRAM) units, each with a capacity of 18 kilobits (Kb), abbreviated as BRAM_18K. In other words, the entire chip has only 15.6 Mb of memory available for storing data, which severely limits the size of the computational system. Additionally, the chip features

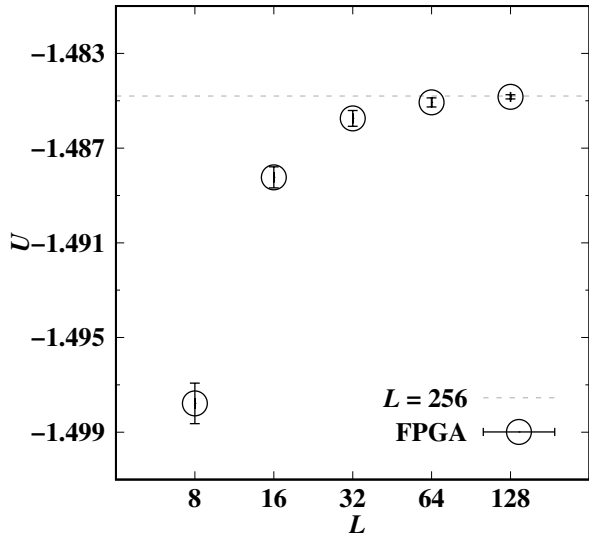


FIG. 5. The internal energy of a single spin in the XY model calculated on FPGA. The black hollow circles represent the numerical values of the internal energy for different L , with error bars indicating a 95% confidence interval. The dashed horizontal reference line represents the average internal energy per spin in a system with $L = 256$ computed using the CPU.

840 Digital Signal Processing slices of the 48E version (DSP48E), 407,600 flip-flops (FF), and 203,800 look-up tables (LUT).

In the MC simulation for the XY model with $L=128$, the utilization percentages of BRAM_18K, DSP48E, FF, and LUT are 42%, 39%, 5%, and 18%, respectively. In the iTEBD calculation for the Heisenberg chain with $D_b=30$, the utilization percentages of BRAM_18K, DSP48E, FF, and LUT are 42%, 63%, 24%, and 69%, respectively.

The CPU used in this work is the Intel Xeon Gold 6230, with a clock frequency of 2.10 GHz. The CPU computations are performed in one core of the Dell PowerEdge R740 server. In a single-core environment, the peak memory for the MC simulation of $L=128$ XY system can reach 80 Mb, with an average memory of 24 Mb. For the iTEBD calculation of a $D_b=30$ Heisenberg system, both the peak and average memory are 16 Mb.

B. Detail of the MC calculation for the XY model

As indicated by the Hamiltonian in Eq.(1), the 2D classical XY model we studied only has nearest neighbour interaction, and the direction of each spin is confined in $[0, 2\pi)$. We use periodic boundary conditions in the calculation. In step 1, a new angle $\theta'_{\mathbf{x}}$ and a new probabilistic decision factor $p_{\mathbf{x}}$ are generated for each spin, where $\theta'_{\mathbf{x}}$ is sampled from a uniform distribution in $[0, 2\pi)$, and

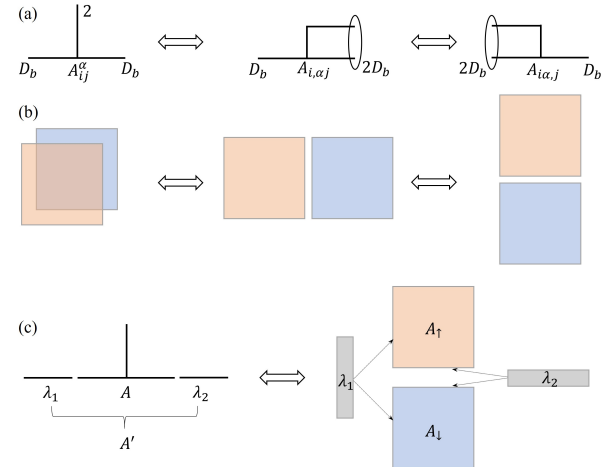


FIG. 6. The different representations of tensor reshaping operations. (a) demonstrates the transformation of a third-order tensor A_{ij}^{α} into two different forms of second-order matrices, (b) depicts the specific configurations of matrix elements corresponding to the transformations, and (c) illustrates the equivalence between the tensor contraction operation $A' = \lambda_1 A \lambda_2$ performed through reshaping on the left and the representation of matrix elements on the right.

$p_{\mathbf{x}}$ is sampled from a uniform distribution in $[0, 1)$. The random number generator is constructed using the linear congruence method. Each spin is initialized with its own unique random seed, enabling each spin to undergo an independent Metropolis process. In step 2, the probability that the spin $S_{\mathbf{x}}$ points in a new direction was calculated as $P(\Delta E_{\mathbf{x}}) = e^{-\beta \Delta E_{\mathbf{x}}}$, where β is the inverse temperature $\frac{1}{T}$, and $\Delta E_{\mathbf{x}}$ is the local internal energy difference caused by the spin rotation,

$$\Delta E_{\mathbf{x}} = - \sum_{\delta} [\cos(\theta'_{\mathbf{x}} - \theta_{\mathbf{x}+\delta}) + \cos(\theta_{\mathbf{x}} - \theta_{\mathbf{x}+\delta})], \quad (4)$$

where δ is a unit vector connecting the site \mathbf{x} with one of its four nearest neighbours. In step 3, probabilistic decision for spin updating is made. If $p_{\mathbf{x}} < P(\Delta E_{\mathbf{x}})$, $\theta_{\mathbf{x}}$ will update to $\theta'_{\mathbf{x}}$. Otherwise, the spin direction will remain unchanged as $\theta_{\mathbf{x}}$.

After dividing the system into two sublattices, the three steps described above can be executed concurrently. This allows each site within one sublattice to evolve independently and in parallel because the system only has nearest neighbor interaction, and the rotation of a spin has no impact on the probability of rotation of another spin in the same sublattice.

We then calculate the internal energy of a single spin for i -th simulation on FPGA, defined as

$$U_i = \frac{1}{L^2} \langle H_{\text{XY}} \rangle \quad (5)$$

where the $\langle \cdot \rangle$ denotes Monte Carlo steps average. Multiple simulations were performed with a series of sizes at temperature $T = 0.85$. Each size had 10 different initial random seeds, resulting in 10 different trajectories

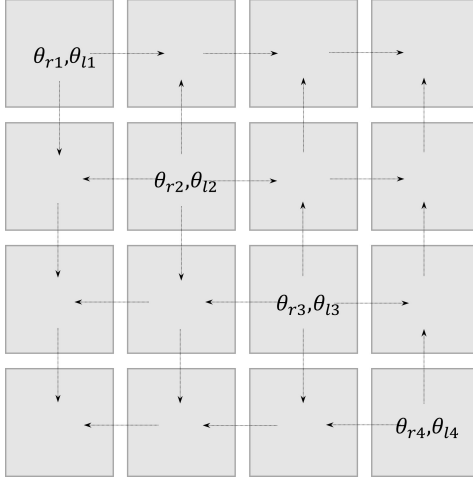


FIG. 7. Two-sided Jacobi rotation (illustrated using an 8x8 matrix as an example), where each square represents a 2×2 matrix. Diagonalization of the four 2×2 matrices on the diagonal squares yields the corresponding left and right rotating angles θ_{li} and θ_{ri} , which are then used to rotate the other 2×2 matrices in the squares.

in phase space. All simulations consisted of 1.2 million Monte Carlo (MC) steps. For each simulation, the last 1 million MC steps were used to measure the average internal energy U_i of the corresponding trajectory, where the subscript i denotes the i -th seed. The final result for the internal energy is calculated as $U = \frac{1}{10} \sum_{i=1}^{10} U_i$. The internal energy U is plotted in Fig. 5. As L increases from 8 to 128, the energy results obtained by FPGA calculations approach more closely to the CPU simulation results for $L = 256$.

C. Detail of the iTEBD calculation for the Heisenberg chain

In the main text, we point out that tensor computations on FPGA need to avoid operations like permutation or reshaping to improve computational efficiency. Here, we need to clarify that the new form of tensor computations in FPGA is equivalent to the old form used in traditional tensor networks, which involves operations like permutation or reshaping. Here, we illustrate this fact with a simple tensor contraction as an example. In the pre-svd step, the matrix $\lambda_{1,2}$ is contracted into the local tensor A or B . We take a A with the dimension $D_b \times D_b \times 2$ for instance [shown in Fig. 6(a)], in a usual tensor network procedure, The tensor A is needed to reshape as a $D_b \times 2D_b$ matrix to connect with λ_1 at the left hand side. After this step is completed, it will reshape to another $2D_b \times D_b$ matrix to connect with λ_2 at the right hand side. Upon careful observation, one can find that tensor reshaping merely involves rearranging the tensor elements, manifesting as fixed blocks of elements appearing at different positions. [shown in Fig. 6(b)]. Therefore,

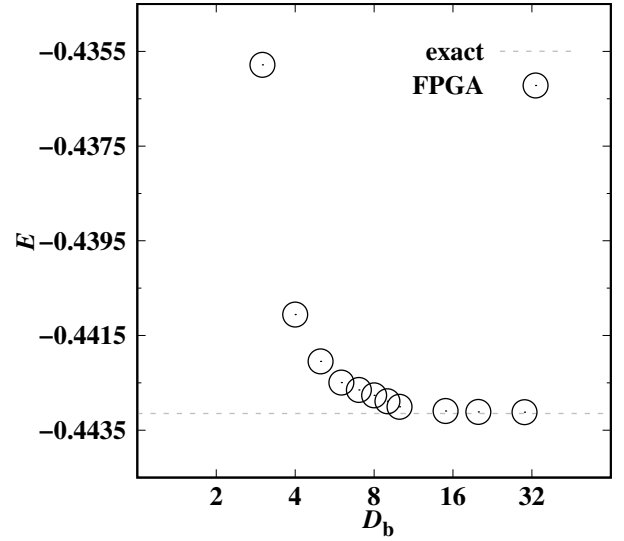


FIG. 8. The average energy of the Heisenberg chain computed from the ground state obtained on FPGA. The black hollow circles represent the energy values for different D_b . The dashed horizontal reference line represents the exact solution, $-\ln 2 + 0.25$.

we can operate on each block of elements A_{\uparrow} or A_{\downarrow} separately instead of operating on the entire tensor A_{ij}^{α} . As the λ s are diagonal, they can be stored as vectors. Then the new quantity A' which connected λ s and A is just [shown in Fig. 6(c)]

$$A'_{\uparrow/\downarrow,ij} = \lambda_{1,i} A_{\uparrow/\downarrow,ij} \lambda_{2,j}. \quad (6)$$

This operation for the tensor elements can be calculated parallelly. In the pre-svd step, other tensor network contraction can be operated similarly, shown in the Fig. 3 in the main text.

Next, in the svd step, one need to obtain the first D_b singular values of a $2D_b \times 2D_b$ matrix M . We use two-sided Jacobi algorithm to perform the SVD calculation $\Lambda = U^{\dagger} M V$. Firstly, we separate the $2D_b \times 2D_b$ matrix M into $D_b \times D_b$ small matrices with dimension 2×2 . This forms a $D_b \times D_b$ block matrix with row and column indice (i, j) . The matrix U (or V) is then the products of left (or right) Jacobi rotation matrice $J_{r/l}$ obtained by diagonalizing the 2×2 blocks in the diagonal direction. At each i , the J_{r_i/l_i} has the form,

$$J_{r_i/l_i} = \begin{bmatrix} \cos \theta_{r_i/l_i} & \sin \theta_{r_i/l_i} \\ -\sin \theta_{r_i/l_i} & \cos \theta_{r_i/l_i} \end{bmatrix} \quad (7)$$

The nondiagonal 2×2 blocks with the row and column indice (i, j) are rotated by the angles θ_{l_i} and θ_{r_j} . Figure 7 shows this procedure with an example of $D_b = 4$.

After one step of the rotation is performed, the matrix M is transformed into a new matrix M' to iterate

the next rotation. The transformation is according to a systolic array [20], where the row/column indice of M changes with the order

$$\begin{aligned} 2i-1 &\rightarrow 2i+1, \\ 2i+2 &\rightarrow 2i \end{aligned}$$

at $1 \leq i \leq D_b - 1$ except for the two boundary cases where $1 \rightarrow 1$, $2 \rightarrow 3$ and $2D_b - 1 \rightarrow 2D_b$. Take $D_b = 4$ for example, start from the ordinary order from one to eight, this systolic array is

$$\begin{aligned} &1, 2, 3, 4, 5, 6, 7, 8; \\ &1, 4, 2, 6, 3, 8, 5, 7; \\ &1, 6, 4, 8, 2, 7, 3, 5; \\ &1, 8, 6, 7, 4, 5, 2, 3; \\ &1, 7, 8, 5, 6, 3, 4, 2; \\ &1, 5, 7, 3, 8, 2, 6, 4; \\ &1, 3, 5, 2, 7, 4, 8, 6; \end{aligned}$$

After seven steps, the array goes back to the ordinary order. By using this systolic array, all the possible combinations of the 2×2 blocks are considered. Iterating these procedure will converge the Matrix M into a diagonal form. The new λ_2 is the singular values of the matrix M . In the post-svd step, the new $A_{\uparrow/\downarrow}$ or $B_{\uparrow/\downarrow}$ can be calculated by contracting λ_1^{-1} into the matrice U and V . the iTEBD iteration is operated to $A_{\uparrow/\downarrow}$, $B_{\uparrow/\downarrow}$ and λ_1 , λ_2 alternately, until the ground state $|\Psi\rangle$ is obtained.

The ground state energy per bond for the Heisenberg chain is then calculated by

$$E = \langle \Psi | H_{ij} | \Psi \rangle / \langle \Psi | \Psi \rangle \quad (8)$$

The energy result at different D_b from the ground state obtain from the FPGA is shown in Fig. 8. As D_b is increased, it is converged into the exact result.

[1] A. W. Sandvik, Computational studies of quantum spin systems, in *AIP Conference Proceedings* (AIP, 2010).

[2] S. R. White, Density matrix formulation for quantum renormalization groups, *Phys. Rev. Lett.* **69**, 2863 (1992).

[3] J. I. Cirac, D. Pérez-García, N. Schuch, and F. Verstraete, Matrix product states and projected entangled pair states: Concepts, symmetries, theorems, *Rev. Mod. Phys.* **93**, 045003 (2021).

[4] Y. Meurice, R. Sakai, and J. Unmuth-Yockey, Tensor lattice field theory for renormalization and quantum computing, *Rev. Mod. Phys.* **94**, 025005 (2022).

[5] J. L. Patterson, David A; Hennessy, *Computer Organization and Design: The Hardware/Software Interface*, 5th ed., The Morgan Kaufmann Series in Computer Architecture and Design (Morgan Kaufmann Publishers, 2013).

[6] J. Backus, Can programming be liberated from the von neumann style?: a functional style and its algebra of programs, *Communications of the ACM* **21**, 29 (1978).

[7] I. L. Markov, Limits on fundamental limits to computation, *Nature* **512**, 147 (2014).

[8] A. Morningstar, M. Hauru, J. Beall, M. Ganahl, A. G. Lewis, V. Khemani, and G. Vidal, Simulation of quantum many-body dynamics with tensor processing units: Floquet prethermalization, *PRX Quantum* **3**, 020331 (2022).

[9] J. M. Rodríguez-Borbón, A. Kalantar, S. S. R. K. C. Yamjala, M. B. Oviedo, W. Najjar, and B. M. Wong, Field programmable gate arrays for enhancing the speed and energy efficiency of quantum dynamics simulations, *Journal of Chemical Theory and Computation* **16**, 2085 (2020).

[10] S. Mittal, A survey of fpga-based accelerators for convolutional neural networks, *Neural Computing and Applications* **32**, 1109 (2018).

[11] PandaX-Collaboration, Limits on the luminance of dark matter from xenon recoil data, *Nature* **618**, 47 (2023).

[12] H. Lv, N. Xie, M. Li, M. Dong, C. Sun, Q. Zhang, L. Zhao, J. Li, X. Zuo, H. Chen, F. Wang, and C. Fan, Dna-based programmable gate arrays for general-purpose dna computing, *Nature* **622**, 292 (2023).

[13] F. Ortega-Zamorano, M. A. Montemurro, S. A. Cannas, J. M. Jerez, and L. Franco, Fpga hardware acceleration of monte carlo simulations for the ising model, *IEEE Transactions on Parallel and Distributed Systems* **27**, 2618 (2016).

[14] C. Yoshimura, M. Hayashi, T. Okuyama, and M. Yamamoto, Fpga-based annealing processor for ising model, in *2016 Fourth International Symposium on Computing and Networking (CANDAR)* (IEEE, 2016).

[15] M. Baity-Jesi, R. Baños, A. Cruz, L. Fernandez, J. Gil-Narvion, A. Gordillo-Guerrero, D. Iñiguez, A. Maíorano, F. Mantovani, E. Marinari, V. Martin-Mayor, J. Monforte-García, A. M. n. Sudupe, D. Navarro, G. Parisi, S. Perez-Gaviro, M. Pivanti, F. Ricci-Tersenghi, J. Ruiz-Lorenzo, S. Schifano, B. Seoane, A. Tarancon, R. Tripiccione, and D. Yllanes, The janus project: boosting spin-glass simulations using fpgas, *IFAC Proceedings Volumes* **46**, 227 (2013).

[16] Q. Zhai, I. Paga, M. Baity-Jesi, E. Calore, A. Cruz, L. A. Fernandez, J. M. Gil-Narvion, I. Gonzalez-Adalid Pe-martin, A. Gordillo-Guerrero, D. Iñiguez, A. Maíorano, E. Marinari, V. Martin-Mayor, J. Moreno-Gordo, A. Muñoz Sudupe, D. Navarro, R. L. Orbach, G. Parisi, S. Perez-Gaviro, F. Ricci-Tersenghi, J. J. Ruiz-Lorenzo, S. F. Schifano, D. L. Schlagel, B. Seoane, A. Tarancon, R. Tripiccione, and D. Yllanes, Scaling law describes the spin-glass response in theory, experiments, and simulations, *Phys. Rev. Lett.* **125**, 237202 (2020).

[17] G. Vidal, Classical simulation of infinite-size quantum lattice systems in one spatial dimension, *Phys. Rev. Lett.* **98**, 070201 (2007).

[18] J. M. Kosterlitz and D. J. Thouless, Ordering, metastability and phase transitions in two-dimensional systems,

Journal of Physics C: Solid State Physics **6**, 1181 (1973).

[19] Y. Kim, A. Eddins, S. Anand, K. X. Wei, E. van den Berg, S. Rosenblatt, H. Nayfeh, Y. Wu, M. Zaletel, K. Temme, and A. Kandala, Evidence for the utility of quantum computing before fault tolerance, *Nature* **618**, 500 (2023).

[20] F. T. Luk, A parallel method for computing the generalized singular value decomposition, *Journal of Parallel and Distributed Computing* **2**, 250 (1985).

[21] S. Zhang, X. Tian, C. Xiong, J. Tian, and D. Ming, Fast implementation for the singular value and eigenvalue decomposition based on fpga, *Chinese Journal of Electronics* **26**, 132 (2017).

[22] Y. Liu, S. Lv, Y. Yang, and H. Zou, Signatures of quantum criticality in the complex inverse temperature plane, *Chinese Physics Letters* **40**, 050502 (2023).

[23] W.-Y. Liu, S.-S. Gong, Y.-B. Li, D. Poilblanc, W.-Q. Chen, and Z.-C. Gu, Gapless quantum spin liquid and global phase diagram of the spin-1/2 j_1 - j_2 square antiferromagnetic heisenberg model, *Science Bulletin* **67**, 1034 (2022).

[24] H. Zou, F. Yang, and W. Ku, Nearly degenerate ground states of a checkerboard antiferromagnet and their bosonic interpretation, *Sci. China Phys. Mech. Astron.* **67**, 10.1007/s11433-023-2190-5 (2023).